Available online at www.sciencedirect.com
SCIENCE DIRECT®
PERGAMON
Solid State Communications 128 (2003) 461–466
solid state communications
www.elsevier.com/locate/ssc

Optical properties of $Zn_{0.5}Cd_{0.5}Se$ thin films grown on InP by molecular beam epitaxy

O. Maksimov[a,*], W.H. Wang[a], N. Samarth[a], Martin Muñoz[b], M.C. Tamargo[b]

[a]*Department of Physics, Pennsylvania State University, 104 Davey Lab, University Park, PA 16802, USA*
[b]*Department of Chemistry, City College of New York, New York, NY 10031, USA*

Received 14 July 2003; received in revised form 12 August 2003; accepted 13 August 2003 by E.L. Ivchenko

Abstract

We report photoluminescence (PL) and reflectivity measurements of $Zn_{0.5}Cd_{0.5}Se$ epilayers grown by molecular beam epitaxy on InP substrates. The low-temperature PL spectra are dominated by asymmetric lines, which can be deconvoluted into two Gaussian peaks with a separation of ~8 meV. The behavior of these peaks is studied as a function of excitation intensity and temperature, revealing that these are free exciton (FE) and bound exciton emission lines. Two lower energy emission lines are also observed and assigned to the first and second longitudinal optical phonon replicas of the FE emission. The temperature dependence of the intensity, line width, and energy of the dominant emission lines are described by an Arrhenius plot, a Bose–Einstein type relationship, Varshni's and Bose–Einstein equations, respectively.

PACS: 78.30.Fs; 78.40.Fy; 78.55.Et

Keywords: A. ZnCdSe; B. MBE; E. Photoluminescence

1. Introduction

There is a significant technological interest in light emitting and laser diodes (LEDs and LDs) operating in the blue–green regions of the spectrum. The possible areas of application include high-density data storage, fiber-optical communication, projection displays, xerography, and medical imaging. Significant success has been recently achieved with the group III-nitride semiconductor material family and pure-blue $Al_xGa_yIn_{1-x-y}N$-based LDs were developed to the stage of practical use [1]. However, to shift the emission to the longer wavelength region, it is necessary to increase the In content of the quantum well (QW) region. This introduces serious In compositional fluctuations and phase separation and results in a gain broadening, rapid increase in threshold current density, and the fast degradation of the device [2]. Since $Al_xGa_yIn_{1-x-y}P$-based LDs operate only below 600 nm, there is a spectral gap in the green–yellow region (530–590 nm) for all commercially available devices. This spectral region is important for many emerging technologies, such as the use of plastic-optical fibers that require green lasers to achieve the lowest attenuation coefficient [3]. Together with the recent improvements in the degradation stability, this revises interest in ZnSe-based LDs that can potentially cover the whole green spectral region (490–590 nm) [4].

$Zn_xCd_{1-x}Se$ alloy is commonly used as a QW material in the ZnSe-based diodes. With $x = 0.5$, $Zn_xCd_{1-x}Se$ is of special interest, since at this composition it is lattice matched to InP substrate and can be used as a QW layer in the totally lattice-matched $Zn_xCd_yMg_{1-x-y}Se$ [5], $Zn_xMg_{1-x}Se_yTe_{1-y}$ [6], and $Zn_xBe_{1-x}Te$ [7]-based light emitters. Since these structures are grown totally lattice matched or pseudomorphic, they are expected to be more reliable and less prone to degradation. Furthermore, they can be combined in a single epitaxial growth process with highly reflective $Zn_xCd_yMg_{1-x-y}Se$-based distributed Bragg reflectors [8], making possible the development of

* Corresponding author. Tel.: +1-814-863-9514; fax: +1-814-865-3604.
E-mail address: maksimov@netzero.net (O. Maksimov).

0038-1098/$ - see front matter © 2003 Elsevier Ltd. All rights reserved.
doi:10.1016/j.ssc.2003.08.011

vertical cavity surface emitting lasers and other microcavity structures. Finally, we note that high quality ZnSe-based epitaxial layers and quantum wells are also important in the context of spin-based quantum information processing schemes since these materials exhibit relatively long spin coherence times (a few nanoseconds) even at room temperature [9].

In this work, we use photoluminescence (PL) and reflectivity to investigate the optical properties of high-quality $Zn_{0.5}Cd_{0.5}Se$ epilayers grown on InP. The low temperature PL spectra show various band-edge emission peaks including bound and free excitons (BE and FE). Longitudinal optical (LO) phonon replicas of the FE emission are also observed, indicating high crystalline quality of the epilayer. The temperature dependence of the PL emission is studied in the range from 4.2 to 300 K. From the Arrhenius plots of the integrated intensity as a function of the inverse temperature, activation energies for the PL emission are estimated. The broadening of the PL emission line width with temperature is also analyzed and found to be mostly due to the LO phonon and impurity scattering. The temperature dependence of the emission energy, an important parameter for design of LDs and LEDs, is fit to the Varshni and Bose–Einstein equations.

2. Experimental details

Two $Zn_{0.5}Cd_{0.5}Se$ epilayers (A and B) were grown on semi-insulating epi-ready InP (100) substrates using elemental Zn, Cd, and Se sources in a Riber 2300P MBE system consisting of III–V and II–VI growth chambers connected by an ultra-high vacuum transfer channel. The InP substrates were first deoxidized in the III–V chamber by heating to 480 °C in the presence of an As flux impinging on the InP surface, A lattice matched $In_{0.5}Ga_{0.5}As$ buffer layer (170 nm) was grown after the deoxidization. Then, the wafers were transferred in vacuum to the II–VI chamber for the $Zn_{0.5}Cd_{0.5}Se$ growth. Immediately after the transfer, the wafers were heated to 170 °C and the III–V surface was exposed to a Zn flux for 30 s (Zn-irradiation) followed by the growth of 10 nm of a low-temperature (170 °C) $Zn_{0.5}Cd_{0.5}Se$ interfacial layer. Then, the growth was interrupted and the growth temperature was increased to 270 °C. $Zn_{0.5}Cd_{0.5}Se$ growth was performed at 270 °C under Se-rich conditions with the growth rate of 0.5 μm/h. These steps have previously been shown to produce high quality $Zn_xCd_{1-x}Se$ layers [10].

The growth mode and surface reconstruction were monitored in situ by reflection high-energy electron diffraction (RHEED). Lattice constants were measured by double-crystal X-ray diffraction (XRD) using Cu $K_{\alpha 1}$ radiation. XRD measurements showed that the epilayers were slightly mismatched to the InP substrate [$\Delta a/a_0 = -0.21\%$(A) and $\Delta a/a_0 = -0.14\%$(B)] and the full width at half maximum (FWHM) of the X-ray rocking curves was around 50 arcsec, indicating high crystalline quality. The alloy composition was estimated from the lattice constant, assuming the validity of Vegard's law and using 6.05 and 5.67 Å as the lattice constants of CdSe and ZnSe, respectively [11].

PL measurements were performed in a liquid He continuous flow cryostat in the temperature range from 4.2 to 300 K. The 488-nm line of an Ar ion laser was used for excitation. The collected PL was spectrally resolved by a monochromator and detected by a cooled charge coupled device (CCD) array detector. The spectral resolution of the system was around 0.1 meV. Reflectivity measurements were performed in the same cryostat using a 200-W Hg lamp.

3. Results and discussion

Low-temperature (4.2 K) PL (solid line) and reflectivity (dotted line) spectra of $Zn_{0.5}Cd_{0.5}Se$ are shown in Fig. 1. The PL spectrum is dominated by a sharp and narrow emission line (E) centered at 2.177 eV. The exciton absorption occurs at around 2.183 eV, as indicated by the sharp line just above Fabry–Perot oscillations in the reflectivity spectrum. This indicates that near-band-edge emission is observed in the PL spectrum. The same PL emission line is shown in a log scale in Fig. 2. It has an asymmetric line shape with a tail at a high-energy side. This

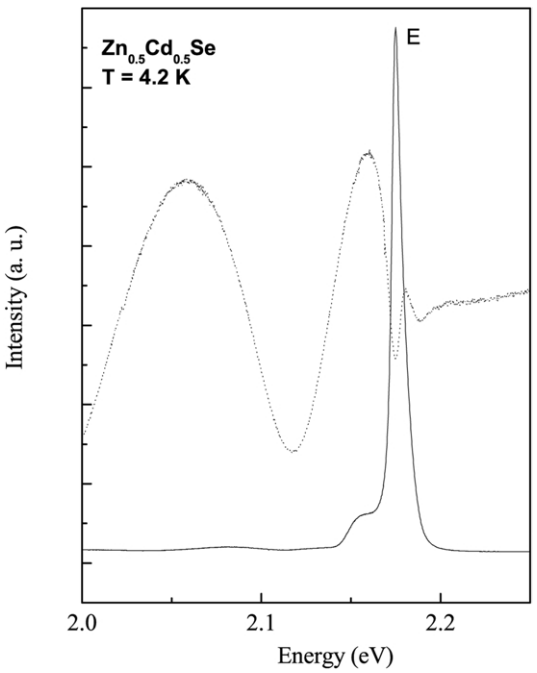

Fig. 1. Photoluminescence (solid line) and reflectivity (dotted line) spectra of $Zn_{0.5}Cd_{0.5}Se$ taken at 4.2 K.

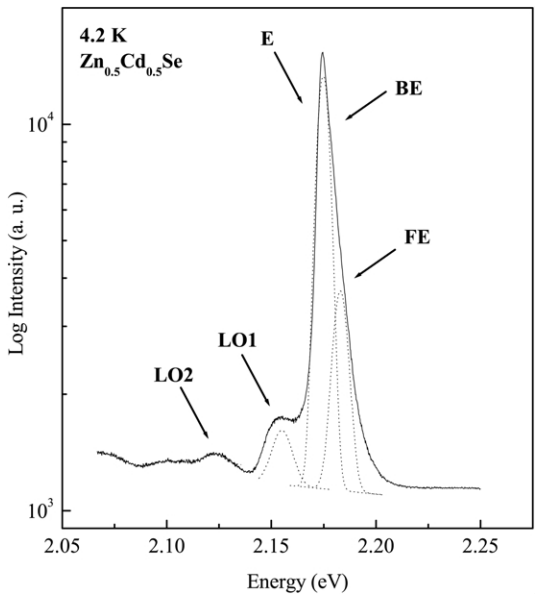

Fig. 2. Photoluminescence spectrum of $Zn_{0.5}Cd_{0.5}Se$ taken at 4.2 K. Solid line is the experimental spectrum and dotted lines are the Gaussian deconvolution.

line can be decomposed into two Gaussian-shape peaks with centers at 2.183 and 2.175 eV. Also, two weaker and broader peaks at 2.155 and 2.123 eV are observed.

We elucidate the origin of the higher energy emission lines (2.175 and 2.183 eV) by studying the dependence of the emission intensity on the excitation laser density. A linear dependence with a slope near unity ($k = 1.04$ for 2.175 peak and 1.08 for 2.183 eV peak) is obtained, as shown in Fig. 3. Also, we do not observe any shift of the emission energy as a function of the excitation laser density. This behavior is consistent with the excitonic origin of the emission.

The separation between the two higher energy emission lines is around 8 meV: this is of the order of the localization energy of the neutral donor BE in the II–VI alloys. For example, in ZnSe:Cl epilayers the neutral donor BE

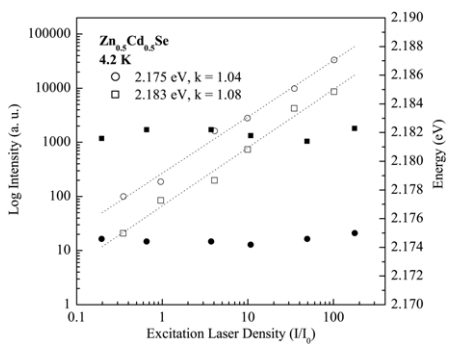

Fig. 3. Dependence of the emission intensity (open symbols) and emission energy (solid symbols) on the excitation laser density at 4.2 K in a log scale. The dashed lines are linear fits.

emission is observed at 2.797 eV, 6 meV below the FE emission [12]. Hence, we attribute the high energy and low energy PL transitions to FE and impurity BE, respectively.

We plot the integrated intensity of deconvoluted FE and BE emission lines as a function of temperature in Fig. 4. For convenience and to avoid the use of absolute intensities (A), the integrated intensity (I) is defined as:

$$I_J(T) = A_J(T)/(A_{FE}(T) + A_{BE}(T)) \quad J = FE, BE \tag{1}$$

The integrated intensity of the FE emission (solid circles) increases with temperature, while the integrated intensity of BE emission (open circles) decreases. The emission intensity is proportional to the population density that can be described as $\sim [1 - \exp(-\Delta E/k_B T)]$ for BEs and $\sim [1 + \exp(-\Delta E/k_B T)]$ for FEs, where ΔE is the exciton localization energy. Therefore, the increase in the integrated intensity of FE emission agrees with the increase in FE population due to the thermally activated dissociation of BE into FE. The best fit (shown with dotted lines) gave us $\Delta E = 6.7 \pm 0.5$ meV, that is close to the localization energy of the neutral donor BE and is in agreement with our previous results.

The two lower energy emission lines are displaced by 28 and 60 meV from the FE emission line. This separation is comparable to the LO phonon energy previously reported for $Zn_{0.56}Cd_{0.44}Se$ alloy (28.7 meV) [13]. Hence, these lines are identified as the first and second LO phonon replicas of the FE line.

The intensity of the dominant PL emission line (E) is shown as an Arrhenius plot in Fig. 5. The experimental data (solid circles) are fit to a model involving two non-radiative recombination processes (solid lines) [14,15]:

$$I(T) = I_0/(1 + C_1 \exp(-E_{A1}/k_B T) + C_2 \exp(-E_{A2}/k_B T)) \tag{2}$$

where I_0, C_1, and C_2 are constants, T is the temperature of

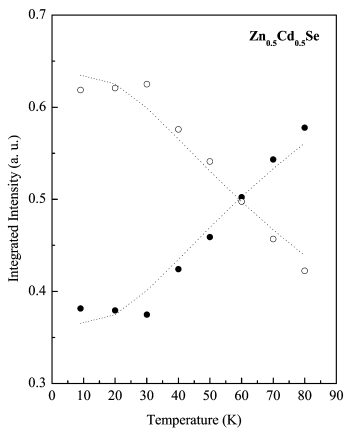

Fig. 4. Dependence of the integrated intensity of FE (solid circles) and BE (open circles) emission lines as a function of temperature. The dashed lines are the fits.

the sample, k_B is the Boltzmann's constant, E_{A1} and E_{A2} are the activation energies. Activation energies of 27.2 and 7.8 meV are obtained from this fit (Table 1). The activation energy of 27.2 meV corresponds to the thermal dissociation of FE and is in good agreement with the average value of exciton binding energy in ZnSe and CdSe (35.9 and 11.6 meV, respectively) [11]. The activation energy of 7.8 meV is in agreement with the energy difference between FE and BE emission lines. Therefore, it corresponds to the thermal activation of BEs to FEs.

Fig. 6 shows the FWHM of the dominant PL emission line (E) versus temperature. The measured luminescence line width is the sum of an inhomogeneous part (Γ_i) that is due to the intrinsic effects (dislocations, interface roughness, composition fluctuations, alloy scattering, and electron–electron interactions), and a temperature-dependent homogeneous part (Γ_h). At low temperatures, the homogeneous component is dominated by the scattering of acoustical phonons (AC). As the temperature increases, the LO phonon scattering becomes dominant due to the increase of phonon population. The broadening due to the impurity scattering also becomes important at higher temperatures due to the ionization of impurities. Based on the above description, the FWHM of the emission line can be expressed through the following equations [16,17]:

$$\Gamma(T) = \Gamma_i + \Gamma_h \tag{3}$$

$$\Gamma_h = \Gamma_{AC}T + \Gamma_{LO}/(\exp(E_{LO}/k_BT) - 1) + \Gamma_{imp}/(\exp(E_{imp}/k_BT)) \tag{4}$$

where Γ_i and Γ_h are inhomogeneous and homogeneous broadening; Γ_{AC}, Γ_{LO}, and Γ_{imp} are the interaction constants; E_{LO} and E_{imp} are the average LO phonon energy and the impurity ionization energy. Using the average value of Γ_{LA} for CdSe and ZnSe (0.001 meV/K) [18] and keeping Γ_i a fixed parameter (the measured at 4.2 K line width), the best fit (solid line) gave us $\Gamma_{LO} = 62$ meV, $E_{LO} = 30$ meV and $\Gamma_{imp} = 15$ meV, $E_{imp} = 9.3$ meV (Table 2). The strength of the electron (exciton)–LO phonon interaction is an important parameter since it affects optical and electrical properties of semiconductors (emission line broadening, hot carriers cooling, carrier mobility). Therefore, it is interesting to compare the value of electron (exciton)–LO phonon interaction in $Zn_{0.5}Cd_{0.5}Se$ with those in other wide band gap semiconductors. The following Γ_{LO} values were reported: 17 meV for CdTe [18], 41 meV for CdS [18], 81 meV for ZnSe [19], 49 meV for CdSe [20], 876 meV for ZnO [21], and 525 meV for GaN [22]. The value of electron (exciton)–LO phonon interaction in $Zn_{0.5}Cd_{0.5}Se$ is comparable to the values reported for the II–S, Se, Te-based semiconductors and significantly smaller the values reported for oxides and nitrides. Therefore, we expect that the high temperature performance of the devices based on $Zn_xCd_{1-x}Se$ materials will be significantly less affected by the electron (exciton)–LO phonon interaction than the performance of the devices based on the $Al_xGa_y In_{1-x-y}N$ and $Zn_xMg_{1-x}O$ alloys.

The estimated value of the impurity ionization energy (9.3 meV) is comparable to the previously reported for CdSe (9.4 meV) [20] and reasonable for shallow donors in II–VI alloys. For example, the ionization energy of persistent donor in ZnTe was estimated to be around 17.4 meV [23].

Table 1
Parameters used to fit temperature dependence of emission intensity

Material	E_{A1} (meV)	E_{A2} (meV)
$Zn_{0.5}Cd_{0.5}Se$ (A)	24.2 (3.4)	8.4 (0.9)
$Zn_{0.5}Cd_{0.5}Se$ (B)	30.1 (3.9)	7.2 (0.6)
Average	27.2	7.8

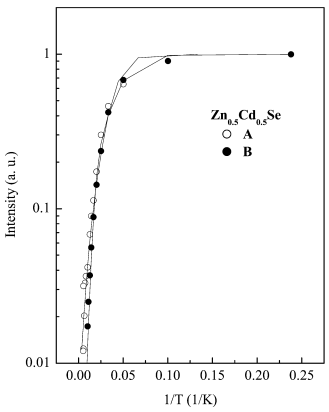

Fig. 5. Arrhenius plot of the emission intensity versus inverse temperature. The solid lines are the fit to the scattered experimental data using the two-step quenching model.

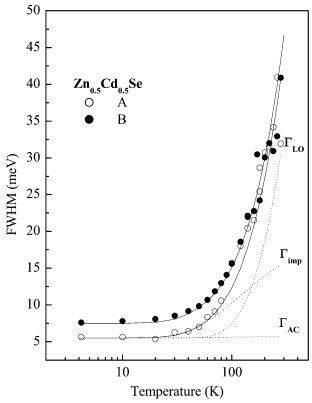

Fig. 6. Temperature dependence of the linewidth (FWHM) of the emission. The circles show the experimental data and the solid lines are obtained by fitting to the following equation: $\Gamma(T) = \Gamma_0 + \Gamma_{AC}T + \Gamma_{LO}/(\exp(E_{LO}/k_BT) - 1) + \Gamma_{imp}/(\exp(E_{imp}/k_BT))$. The dotted lines demonstrate contributions from the scattering with the acoustical phonons, longitudinal optical phonons, and ionized impurities.

Table 2
Parameters used to fit temperature dependence of emission broadening

Material	Γ_0	Γ_A	Γ_{LO}	E_{LO}	Γ_{imp}	E_{imp}
$Zn_{0.5}Cd_{0.5}Se$ (A)	5.5	0.001	62	30	15	10
$Zn_{0.5}Cd_{0.5}Se$ (B)	7.5	0.001	62	30	15	8.6
Average	6.5	0.001	62	30	15	9.3

Since $Zn_{0.5}Cd_{0.5}Se$ and ZnTe have similar values of static dielectric constants [11], comparable ionization energies are expected. Chlorine forms a shallow donor in the II–VI alloys and a $ZnCl_2$ effusion cell was installed in the MBE growth chamber and routinely used for *n*-type doping. Therefore, it is plausible to think that chlorine was a residual impurity in the layers.

The individual contributions of the AC phonons, LO phonons, and ionized impurities to the FWHM of the emission line from the sample A are also shown in Fig. 6 by the dotted lines. The contribution from the scattering of AC phonons is important at low temperatures, but does not have significant contribution at high temperatures, while the broadening due to the LO phonon scattering dominates at the higher temperatures. The broadening due to the impurity scattering also strongly influence the FWHM of the emission line (especially at around 100 K) and should not be neglected.

The dependence of the energy of the dominant PL emission line (E) and absorption edge (estimated through reflectivity measurements) on temperature are shown in Fig. 7, where symbols represent the experimental results. The data is fit to the Bose–Einstein type relationship (solid lines) [24]:

$$E_{BE}(T) = E(0) - 2a_B/(\exp(\theta/T) - 1) \quad (5)$$

where $E(0)$ is the energy of the transition at 0 K, a_B represents the strength of the electron-average phonon interaction, and θ corresponds to the average phonon temperature. The (best) fit yields $E_0 = 2.175$ eV, $a_B = 21$ meV and $\theta = 136$ K for the PL emission energy (Table 3) and $E_0 = 2.182$ eV, $a_B = 22$ meV and $\theta = 155$ K for the absorption edge (Table 4). A good correlation between the parameters obtained by two different techniques shows that the emission line follows the absorption edge over the whole temperature range.

The estimated average phonon temperature is significantly lower than the average LO phonon temperature calculated from the emission line broadening (~350 K), indicating that acoustic as well as optical phonons contribute to the red-shift of the emission energy.

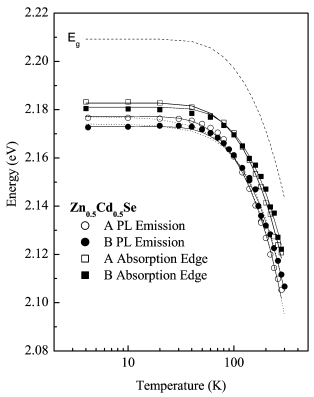

Fig. 7. Temperature dependence of the energy of dominant emission line (E) and absorption edge. Symbols correspond the experimental data, solid and dotted lines show the fits based on the Bose–Einstein and Varshni's equations, dashed line shows the temperature dependence of $Zn_{0.5}Cd_{0.5}Se$ band gap.

The experimental PL emission energy is also fit to the more widely used Varshni's semi-empirical relationship (dotted lines) [25]:

$$E_V(T) = E(0) - \alpha T^2/(\beta + T) \quad (6)$$

where $E(0)$ is the transition energy at 0 K and α and β are constants, known as Varshni's coefficients. Although the Bose–Einstein equation provides a better description of the data at low temperature, both equations agree quite well at the high temperature limit [26,27]. The Varshni's fit yields $E_0 = 2.175$ eV, $\alpha = 0.37$ meV/K and $\beta = 141$ K (Table 3). These values are in reasonable agreement with the values reported by Lo et al. for $Zn_{0.8}Cd_{0.2}Se$ (0.40 meV/K and 133 K) [28], by Malikova et al. for $Zn_{0.56}Cd_{0.44}Se$ (0.45 meV/K and 153 K) [12], and by Lunz et al. for the same $Zn_xCd_{1-x}Se$ composition (0.49 meV/K and 180 K) [29].

The band gap energy of $Zn_{0.5}Cd_{0.5}Se$ is determined over the entire temperature range by adding the exciton binding energy (27.2 meV) to the energy of the exciton absorption. The estimate is shown in Fig. 7 with dashed line. It should be noted, that our values agree quite well with the 5 K band gap calculated through the equation developed by Brasil

Table 3
Parameters used to fit temperature dependence of emission energy

Material	$E(0)$ (eV)	$2a_B$ (meV)	θ (K)	α (meV/K)	β (K)
$Zn_{0.5}Cd_{0.5}Se$ (A)	2.177	42 (6)	124 (13)	0.39 (0.03)	126 (27)
$Zn_{0.5}Cd_{0.5}Se$ (B)	2.173	43 (4)	148 (19)	0.35 (0.02)	155 (20)
Average	2.175	42.5	136	0.37	141

Table 4
Parameters used to fit temperature dependence of absorption edge energy

Material	$E(0)$ (eV)	$2a_B$ (meV)	θ (K)
$Zn_{0.5}Cd_{0.5}Se$ (A)	2.183	43 (5)	144 (13)
$Zn_{0.5}Cd_{0.5}Se$ (B)	2.181	46 (6)	166 (15)
Average	2.182	44.5	155

et al. (2.213 eV) [30], the 10 K band gap measured by Samarth et al. (2.192 eV) [31], and the room temperature band gap calculated through the equation developed by Kim et al. (2.10 eV) [32]. (Spectral conductivity, piezo modulated reflectivity, and spectral ellipsometry were used to measure band gap in the first, second and third cases, respectively). The observed discrepancy in the results can be explained by the errors in the composition measurements (1% change in composition results in a 12 meV shift), errors in the band gap measurements due to the onset of below band gap (Urbach) absorption and interference patterns, and band gap modification by strain.

4. Conclusion

We have studied the optical properties of $Zn_{0.5}Cd_{0.5}Se$ epilayers using PL and reflectivity. The low temperature PL spectrum is dominated by FE and BE emission lines. Also, first and second LO phonon replicas of FE line are observed. The temperature dependence of the dominant PL peak intensity is described by a two-step quenching process. The first activation energy agrees well with the exciton binding energy while the second activation energy is close to the extra binding energy needed to bind FE to an impurity center. Analysis of the temperature dependence of the PL emission linewidth yields an electron (exciton)–LO phonon interaction constant of $\sim$62 meV. The temperature dependence of the FE emission provides the temperature-dependence of the $Zn_{0.5}Cd_{0.5}Se$ band gap dependence on temperature.

References

[1] S. Nakamura, et al., Appl. Phys. Lett. 76 (2000) 22.
[2] S. Nakamura, et al., The Blue Laser Diodes, Springer, Berlin, 2000.
[3] A. Weinert, Plastic Optical Fibers: Principles, Components, Installation, Publicis MCD, Erlangen, 1999.
[4] S.V. Ivanov, Phys. Status Solidi A 192 (2002) 157.
[5] M.C. Tamargo, et al., J. Cryst. Growth 214/215 (2000) 1058.
[6] W. Faschinger, J. Nürnberger, Appl. Phys. Lett. 77 (2000) 187.
[7] S.B. Che, et al., Appl. Phys. Lett. 81 (2002) 972.
[8] O. Maksimov, et al., J. Appl. Phys. 78 (2001) 2473.
[9] J.M. Kikkawa, et al., Science 277 (1997) 1284.
[10] L. Zeng, et al., J. Vaccine Sci. Technol. B 17 (1999) 1255.
[11] H.T. Grahn, Introduction to Semiconductor Physics, World Scientific, Singapore, 1999.
[12] S. Wang, et al., J. Cryst. Growth 220 (2000) 548.
[13] L. Malikova, et al., Phys. Rev. B 54 (1996) 1819.
[14] S. Iyer, et al., Phys. Rev. B 47 (1993) 1329.
[15] J.D. Lambkin, et al., Appl. Phys. Lett. 65 (1994) 73.
[16] H.J. Lozykowski, K. Shastri, J. Appl. Phys. 69 (1991) 3235.
[17] T. Li, et al., Phys. Rev. B 46 (1992) 6961.
[18] S. Rudin, et al., Phys. Rev. B 42 (1990) 11218.
[19] A.J. Fischer, et al., Phys. Rev. Lett. 73 (1994) 2368.
[20] G. Perna, et al., J. Luminescence 76 (1998) 534.
[21] T. Makino, et al., Appl. Phys. Lett. 76 (2000) 3549.
[22] A.K. Visnawath, et al., Phys. Rev. B 58 (1998) 16333.
[23] C.X. Shan, et al., J. Vaccine Sci. Technol. A 20 (2002) 1886.
[24] L. Vina, et al., Phys. Rev. B 30 (1984) 1979.
[25] V.P. Varshni's, Physica 34 (1967) 149.
[26] R. Pässler, et al., J. Appl. Phys. 86 (1999) 4403.
[27] O. Maksimov, et al., J. Appl. Phys. 90 (2001) 5135.
[28] I. Lo, et al., Solid State Commun. 120 (2001) 155.
[29] U. Lunz, et al., J. Appl. Phys. 80 (1996) 6861.
[30] M.S.P. Brasil, et al., J. Appl. Phys. 59 (1991) 106.
[31] The band gap of $Zn_xCd_{1-x}Se$ is calculated using the equation: $1.776 + 0.6359(1-x) + 0.3902(1-x)^2$ with coefficients extracted from Fig. 1 in.N. Samarth, H. Luo, J.K. Furdyna, R.G. Alonso, Y.R. Lee, A.K. Ramdas, S.B. Qadri, N. Otsuka, Appl. Phys. Lett. 56 (1990) 1163.
[32] Y.D. Kim, et al., Phys. Rev. B 49 (1994) 7262.